AIAA 2013-4535

Trajectory Prediction Accuracy and Error Sources for Regional Jet Descents

Jeff Henderson* and Robert A. Vivona†
Engility Corporation, Billerica, MA, 01821

Steven M. Green‡
NASA Ames Research Center, Moffett Field, CA, 94035

The Efficient Descent Advisor (EDA) controller automation tool generates trajectory-based speed, path, and altitude-profile advisories to facilitate efficient, continuous descents into congested terminal airspace. While prior field trials have assessed the trajectory-prediction accuracy for large jet (i.e., Boeing and Airbus) types, smaller (i.e., regional and business) jet types present unique challenges involving different descent procedures and Flight Management System (FMS) capabilities. A small-jet field trial was conducted at Denver in the fall of 2010 with the objective of measuring trajectory prediction accuracy and quantifying the primary sources of error. This paper uses data collected onboard a Bombardier Global 5000 test aircraft to quantify the size and sources of prediction error. Results for en-route descents, from prior to top of descent to the meter fix 60-120 nmi downstream, indicate that the aircraft arrived an average 15 seconds earlier than predicted, with a standard deviation of 10 seconds. Target Mach and CAS deceleration were found to be the two largest error sources. If CAS deceleration error was reduced using a typical, more predictable level flight deceleration then the arrival time prediction error in 2010 would be on par with a 2009 flight trial of Airbus and Boeing revenue flights. Four of the error sources, tracker jumps, CAS deceleration, target Mach, and path distance, lend themselves to significant improvement with modest to no changes to ATC automation and/or procedures. Wind error and its impact on arrival time error was significantly reduced in 2010 compared to a 1994 flight test using NASA's Boeing 737 test aircraft.

I. Introduction

Arrival congestion often inhibits efficient, continuous descent operations at many airports. Current air traffic control (ATC) techniques, without the aid of trajectory-based automation advisories, lead to many corrective changes in speed, path and altitude profiles when controllers attempt to meter arrivals and maintain separation. The Efficient Descent Advisor (EDA)[1-4] is an automation tool that supports controllers with clearance advisories prior to top of descent that are designed to achieve precise meter-fix scheduled times of arrival while enabling continuous descents. Three-Dimensional Path Arrival Management (3D PAM)[3,5-7] is a concept for operational deployment of EDA in advance of data link that leverages EDA automation and the onboard vertical navigation (VNAV) capabilities of flight management systems (FMS). The 3D PAM clearance is designed so that the controller does not need to vector or assign temporary altitudes until the aircraft crosses the meter fix. The ability to fly more efficient speed and altitude profiles reduces fuel burn and emissions and maximizes utilization of the FMS. System benefits include increased flight path predictability and increased arrival-time delivery accuracy at the meter fix.

The 3D PAM descent procedures were validated in a field test involving United and Continental flights arriving at Denver International Airport in the fall of 2009. The mean absolute value of the arrival time error at the meter fix was estimated to be about 12 seconds with wind modeling noted as the main error source[3]. While this and previous field trials focused on large (i.e., Boeing and Airbus) transport types, little attention had been paid to smaller (i.e., regional and business) jet types. Aside from the obvious differences in aircraft performance, the FMS capabilities and descent procedures involve significant differences critical to the accurate prediction of descent trajectories. The

* Senior Research Engineer, AIAA Member
† Chief Research Engineer, AIAA Associate Fellow
‡ Research Scientist, AIAA Associate Fellow

larger types, employing full performance-based VNAV capabilities for planning and executing continuous idle/near-idle descents, typically execute a relatively predictable profile that varies primarily with wind and descent speed. In comparison, the smaller jets employ a simpler FMS with "kinematic" VNAV guidance typically based on a fixed flight-path angle. Moreover, the choice of descent angle is up to the pilot and there exists little standardization in the selection of descent path or pilot procedure.

To fill this gap, a flight trial of 3D PAM small-jet descents was conducted in collaboration with the FAA and Boeing at Denver in the fall of 2010 using a Bombardier Global 5000 flight test aircraft provided by the FAA.* The purpose of this test was threefold: (1) to develop and evaluate procedures in preparation for trials involving revenue flights with a regional carrier; (2) to assess the trajectory prediction accuracy under more controlled conditions; and (3) to collect the airborne data necessary to analyze the source of prediction errors. A prior EDA flight trial[8-9] conducted at Denver in 1994 using a NASA B737 test aircraft using a performance-based FMS VNAV capability found that the dominant error source was predicted winds aloft[10].

The focus of this paper is quantifying the Center-TRACON Automation System (CTAS)[11-13] trajectory prediction accuracy for small-jet descents and to identify and measure the trajectory prediction error sources. Trajectory prediction accuracy is useful for determining the operational viability of the 3D PAM concept in terms of meeting required times of arrival, conflict detection and resolution, and total prediction accuracy, such as the vertical profile, prior to the meter fix. If the trajectory predictions are too inaccurate, then controllers will need to issue additional tactical clearances for separation and conformance to the scheduled time of arrival. Insight into the trajectory prediction error sources could be used to develop techniques to compensate for these errors or to create larger uncertainty buffers used in automation tools. To measure the trajectory prediction accuracy, the CTAS trajectory synthesizer component was used to generate predicted trajectories that were compared to the flown trajectories in the trials. The primary consideration is the predicted time error. Other trajectory prediction accuracy metrics, such as predicted top of descent, bottom of descent, flight path angle, and altitude relative to the flown trajectory are used to describe differences between the predicted and flown trajectories. Seven error sources are identified and quantified based on analysis of radar track along with air data computer (ADC) and global positioning system (GPS) data collected during the flight trial. The contribution of each error source to the time error is quantified along the predicted trajectory from top of descent to the meter fix and aggregated over all the runs.

The paper is organized as follows. Section II describes the Global 5000 3D PAM flight trial at Denver. The quantification of arrival path trajectory prediction accuracy is presented in Section III. Section IV describes seven arrival path trajectory prediction error sources. Section V quantifies the relative magnitude of the seven error sources in terms of their contribution to time error along the descent prediction, and compares the results from this trial to the 1994 NASA B737 trial. Conclusions are then presented in Section VI.

II. Flight Trial

Data for the Global 5000 flight trial was collected between September 27th, 2010 and October 8th, 2010. This section describes the flight trial test matrix, arrival routing, VNAV procedures, and data collection.

A. Test Matrix

A desired test matrix of 45 descent runs was comprised of a primary matrix, involving 36 straight-path descents using speed control, and 9 runs with path stretch and speed control. These descent runs are respectively referred to as direct and path stretch through the remainder of the paper. The Global 5000 aircraft was able to complete 35 of the 36 direct runs and all 9 path stretch runs. One of the runs was scratched, and the desired test matrix was not completed, due conflicting priorities with other flight trial objectives. A summary of the 44 flown runs is shown in Table 1.

Each descent run involved a fixed flight path angle (FPA) descent with a vertical profile anchored at the meter fix crossing restriction and extending back upstream to define the top of descent. For the purpose of this test, the flight crew had the option of selecting one of two pre-defined FPAs depending on the cruise Mach and descent calibrated airspeed (CAS) combinations shown in Table 1. These two FPAs were defined to be consistent with typical descents performed by the FAA pilots in the Global 5000 aircraft. The choice allowed the pilot to pick the angle best suited for the relative winds aloft during that particular run. While the methodology for selecting the FPA would be ambiguous in current-day operations, we assume here that the selection is procedurally defined to ensure that ATC and the supporting automation has accurate knowledge of the planned FPA[14,15]. The right columns of

* A related field trial involving SkyWest Canadair Regional Jet revenue flights will be addressed in a future paper.

Table 1 show the number of flown runs for each FPA for direct and path stretch runs which differ from the desired test matrix.

The goal of the primary matrix was to obtain an even sampling of 9 direct runs each across the four main arrival gates of the Denver TRACON to obtain a balance of headwind and tailwind cases. The four meter fixes (LANDR, RAMMS, QUAIL, and LARKS) correspond to the four arrival gates shown in the leftmost column of Table 1. The 9 runs were comprised of three descent speed profiles, spanning the speed envelope (250, 280 and 300 knots CAS), repeated three times each. The total, which was planned to equal three, was obtained by totaling the runs for each FPA. LANDR is missing one 250 knot descent and there was one extra 280 knot descent into LARKS instead of a 250 knot descent. Of the 9 path stretch test matrix runs planned, three runs for each descent CAS irrespective of meter fix, only two were collected at 250 knots, three at 280 knots, and four at 300 knots.

Table 1. Descent runs by meter fix, CAS, and FPA.

Arrival Gate	Meter Fix	Available Combinations of Mach, CAS and FPA			No. of Runs Flown for each FPA						
					Direct				Path Stretch		
		Cruise Mach	Descent CAS (knots)	Available FPAs	-2.0	-2.5	-3.0	Total	-2.0	-2.5	-3.0
Northeast	LANDR	0.74	250	-2.0, -2.5	2			2	1	1	
		0.76	280	-2.5, -3.0			3	3			
		0.78	300	-2.5, -3.0		1	2	3			2
Northwest	RAMMS	0.74	250	-2.0, -2.5	2	1		3			
		0.76	280	-2.5, -3.0		2	1	3		1	1
		0.78	300	-2.5, -3.0		2	1	3			1
Southeast	QUAIL	0.74	250	-2.0, -2.5		3		3			
		0.76	280	-2.5, -3.0		2	1	3			1
		0.78	300	-2.5, -3.0		1	2	3			
Southwest	LARKS	0.74	250	-2.0, -2.5	1	1		2			
		0.76	280	-2.5, -3.0		3	1	4			
		0.78	300	-2.5, -3.0		1	2	3			1

B. Arrival Routing

The arrival routes for each of the four arrival gates are shown in Fig. 1. Each arrival, both direct (solid black line) and path stretch (dashed black line), begin at a cruising altitude of 30,000 ft to 36,000 ft approximately 95 to 120 nmi from the meter fix. The flight crew then descended the aircraft to the meter fix crossing altitude of 19,000 ft with a deceleration initiated during descent in time to meet the meter fix crossing speed restriction of 250 knots. Once past the meter fix, ATC vectored the aircraft to the next run (grey line) while the aircraft climbed back to the cruising altitude in preparation for the next run. For example, the direct-path arrival route for the northeast arrival gate was initiated at SNY050040 (a position 40 nmi from the Sidney (SNY) VORTAC along the 050^{o} radial), and flown direct LANDR. The corresponding path-stretch route was also initiated at SNY050040 and flown direct SNY140035, direct LANDR. Repositioning the aircraft for another run from the northwest involved vectors to YOKES, then direct COPLA, direct HANKI, direct SNY030045, and direct SNY050040.

C. LNAV/VNAV

During the flight trial, VNAV capability was used for vertical guidance only and was not coupled to the autopilot and autothrottle. VNAV was set up in this way on the Global 5000 to be consistent with the capabilities of the FMS aboard Canadair Regional Jet models 200, 700, and 900. These CRJ models were used for 3D PAM flight trials involving SkyWest airlines that followed the Bombardier Global 5000 runs and will be the subject of another paper.

D. Data Collection

The following subset of ADC and GPS data were automatically recorded during the flight test and used in the identification and quantification of error sources. Time, latitude, longitude, pressure altitude (ADC), and ground-referenced altitude (GPS) were recorded to establish aircraft position. The current aircraft speed was recorded including indicated airspeed (IAS), true airspeed (TAS), Mach, and groundspeed. The Mach or CAS that was being targeted was recorded to establish the target speed. The atmospheric conditions recorded and used in this analysis included wind speed, wind direction, temperature, and air density.

Details of the clearance and other comments were manually recorded onboard and on the ground. Denver Air Route Traffic Control Center (ARTCC) radar track data was recorded at the 12 second radar sweep update rate. Rapid Update Cycle (RUC) atmospheric information was recorded and archived for post-analysis. The EDA initial conditions, rather than the trajectory prediction, were recorded during the flight test to facilitate the generation of the CTAS predicted trajectories during post-processing.

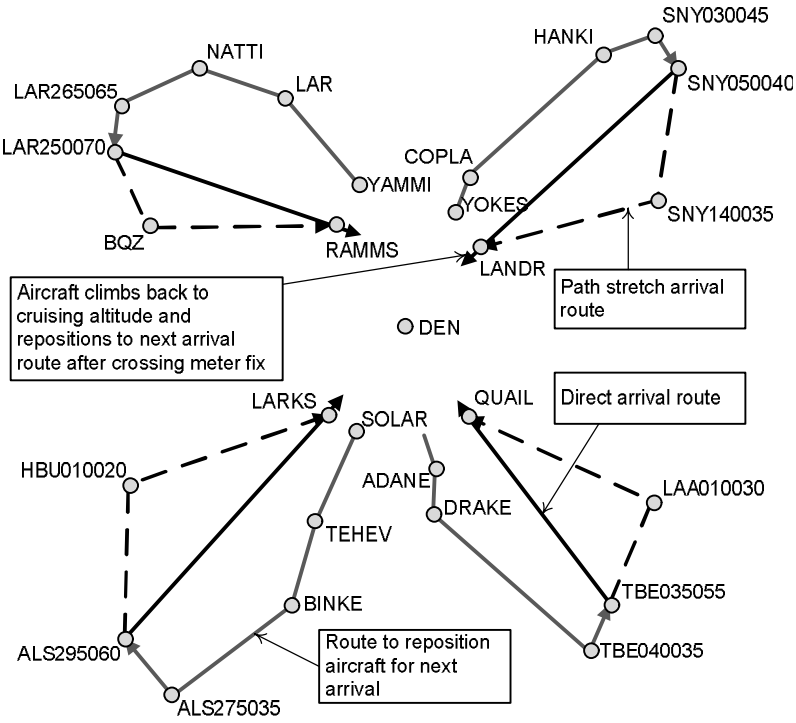

Figure 1. Arrival routes for each of the four Denver arrival gates.

III. Trajectory Prediction Accuracy

This section describes the method to predict the trajectory and its accuracy relative to the flown trajectory.

A. Trajectory Prediction

The trajectory synthesizer component of the CTAS[11-13] was used to generate a 4D trajectory prediction (3D and time) based on the radar track position and groundspeed at each run's initial condition. This initial position was typically 60 to 85 nmi (direct runs) and 100 to 120 nmi (path stretch runs) from the meter fix. The initial condition for direct runs was partway through the arrival route while the initial condition for path stretch runs was at the beginning of the arrival route to account for the path stretch turn. The analysis presented in this paper is based on trajectory predictions run after the field trial had ended using the atmospheric conditions, flight plan, and meter fix crossing restrictions that would have been known to the ground automation system at the start of each run. The trajectory prediction is run once and not updated during the descent to the meter fix.

B. Accuracy

Trajectory prediction accuracy was measured by comparing the recorded radar tracks with the CTAS predicted trajectory. This comparison was based on the spatial location (latitude/longitude) on the predicted trajectory closest to each radar track position. This technique[16] is referred to as closest segment spatial error or spatial correlation.

The distribution of time error at the meter fix across all runs in presented in Fig. 2. Aircraft generally arrived at the fix earlier than predicted as indicated by the negative values along the x-axis in Fig. 2. The trajectory prediction error sources described in Section IV and quantified in Section V will be used to explain this time error.

The mean (-15.4 sec) and standard deviation (10.0 sec) of the time error at the meter fix for direct runs are shown in the left columns of Table 2 along with other

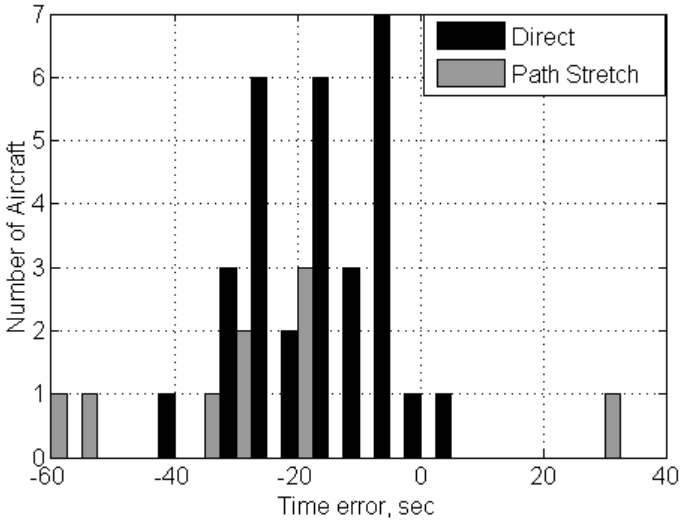

Figure 2. Distribution of time error (flown trajectory – predicted trajectory) at meter fix. A negative value indicates that the aircraft arrived earlier than predicted.

summary statistics. Runs with path stretches shown in the right columns of Table 2 show a significantly larger mean error (-27.0 sec) and standard deviation (25.8 sec) than direct runs.

The top of descent (ii) and bottom of descent (iii) were both 0.3 nmi closer to the meter fix than predicted for direct runs. The relatively small FPA (iv) error (-0.01^o) indicates that the aircraft flew a slightly steeper descent than predicted. The maximum cross-track error (v) is the average of the maximum cross-track error for each of the direct (0.4 nmi cross-track error) and path stretch (2.2 nmi cross-track error) runs. The altitude error (vi) ranged from 30 to 100 ft lower than predicted during direct descents and 100 to 175 ft lower than predicted during path stretch descents.

Table 2. Summary of trajectory prediction errors. μ = mean error and σ = standard deviation of error.

Error Description, units	Direct		Path Stretch	
	μ	σ	μ	σ
i) Time error at meter fix, sec	-15.6	9.9	-27.0	25.8
ii) Top of descent location, nmi	0.3	0.8	0.5	1.0
iii) Bottom of descent location, nmi	0.3	0.4	0.7	0.6
iv) Flight path angle error, deg	-0.01^o	0.04^o	-0.03^o	0.07^o
v) Maximum cross-track error, nmi	0.4	0.2	2.2	0.8
vi) Altitude error				
Top of descent, ft	-116	74	-143	124
Initial condition – 2,000 ft, ft	-63	145	-98	274
Initial condition – 4,000 ft, ft	-34	94	-143	168
Initial condition – 6,000 ft, ft	-34	92	-152	125
Fix altitude + 4,000 ft, ft	-67	121	-158	153
Fix altitude + 2,000 ft, ft	-69	93	-174	185
Bottom of descent, ft	35	115	12	23
Meter fix, ft	35	115	12	23

IV. Error Sources

This section describes seven error sources, labeled A to G in Fig. 3, which were identified and corrected. The white circles along the vertical profile in Fig. 3 correspond to nine reference locations along the predicted trajectory where results were aggregated across all runs. While the bottom of descent and meter fix locations should occur at the same location, they are analyzed separately because of the differences in the actual bottom of descent flown (quantified as the bottom-of-descent location metric in Table 2). These aggregated results are presented in subsections A to G corresponding to the seven error sources.

Error sources are corrected incrementally (i.e., correct for wind and tracker jumps after correcting for tracker jumps only) to isolate the contribution of each error source to the overall trajectory error. For example, comparing a trajectory that has been corrected for wind and tracker jumps against a trajectory that has been corrected for just tracker jumps will estimate the impact of wind errors. Error sources were also corrected cumulatively so that the magnitude of the unexplained residual error can be quantified. Any interactions between error sources will affect the error source magnitudes. Larger interactions between error sources are expected to cause the order that error sources are quantified to become more significant. However, the interactions are relatively small in magnitude as shown by the normalized correlation coefficients included in Tables 4 and 5 in Section V so the focus will be on first-order analysis of error sources.

The tracker jump correction directly alters the time error. The other error corrections, except path distance, correct the groundspeed by replacing predicted components of the groundspeed (wind, TAS, CAS, Mach, temperature, air density) with the observed values recorded by the air data computer. The time error is then derived from the updated CTAS predicted time component along the trajectory. The path distance correction replaces the predicted

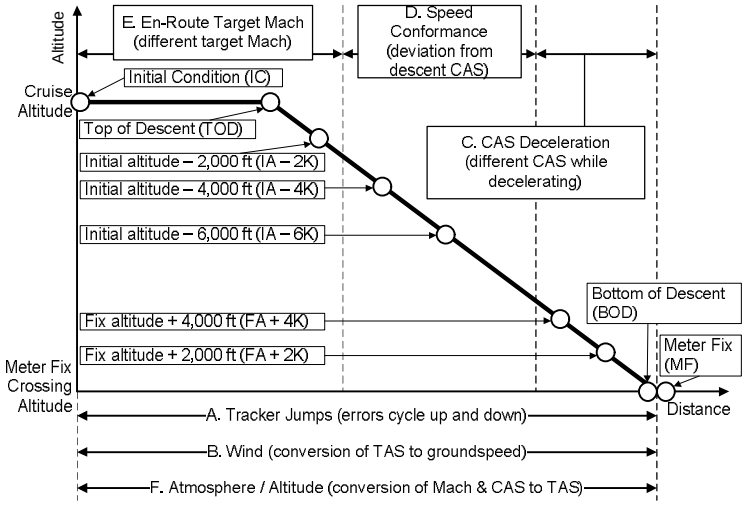

Figure 3. Seven error sources plotted on the vertical profile from the initial condition at cruise altitude to the meter-fix crossing altitude. Also shown are nine reference locations along the predicted trajectory (IC to MF).

distance by the flown distance. In all cases, a convention is adopted that the error equals (-1) * (time error correction magnitude). This method is described in detail in a more extensive companion report[17]. The corrections are made using MATLAB tools to adjust the CTAS predicted trajectory.

A. Tracker Jumps

Tracker jumps, due to truncation of the time component of the En Route Host radar tracker, introduce noise into the time error data. The dashed line in Fig. 4 shows an example of tracker jumps from the second run. The x-axis is the distance along the predicted path starting at the initial condition and ending at the meter fix. The y-axis is the flown time minus the predicted time at the specified distance from the initial condition. The uncorrected curve (dashed line) shows "jumps" of approximately six seconds in the time difference between successive values while the corrected curve (solid line) somewhat mitigates this effect.

The tracker jump error is aggregated across all runs at the nine locations shown along the x-axis of the Fig. 5 box plot. The tracker jump error equals (-1) * (tracker jump correction). The top and bottom whiskers are the minimum and maximum values of the tracker jump error effect. The top and bottom of the box are the first and third quartiles and the line in the box is the median. The median line is not shown at some of the locations since zero second corrections occur about a third of the time causing the median to equal the third quartile. The error due to tracker jumps does not significantly grow in magnitude along the trajectory which will be the case for the other six error sources discussed next.

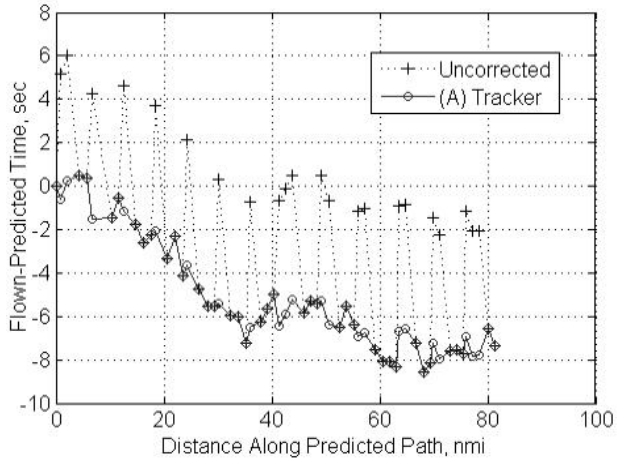

Figure 4. Example tracker jumps from run 2. Solid line has been corrected for tracker jumps while dashed line is uncorrected.

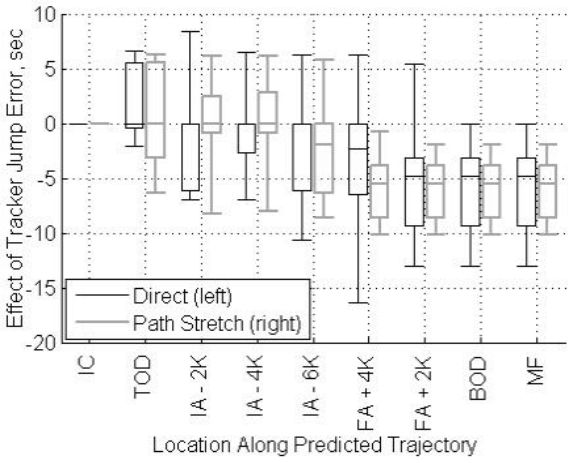

Figure 5. Tracker jump error at locations along predicted trajectory.

B. Wind

There are two sources of errors with respect to the atmospheric model used in the trajectory predictor. One is the difference between winds estimated in the NOAA RUC model and the winds observed by aircraft sensors. Subsection G will describe the second atmospheric model error source, which is the difference between the temperature and pressure estimated by the models and the values sensed by the aircraft. Figure 6 shows an example where the aircraft flew into less of a headwind than expected (negative values along y-axis indicated headwind). The difference between the CTAS predicted winds and winds recorded by the ADC are used to generate the effect of corrected winds on groundspeed in Fig. 7. There is a small wind error (< 5 knots) up to about 40 nmi along the predicted path (about 20 nmi after the top of descent). The wind error then grows to a maximum of about 17 knots over-predicted headwind (i.e., CTAS predicted a stronger headwind than occurred) at about 55 nmi along the predicted path. This difference in predicted vs. actual winds results in about a six second time difference at the meter fix as shown in the Fig. 8 time error plot.

The wind error, which is the difference between the uncorrected and corrected trajectory times, was aggregated to generate the wind error box plot in Fig. 9. Figure 9 shows that there was more of a tailwind (median is negative) than predicted, which caused the aircraft to arrive at the fix earlier than predicted. The wind errors are also cumulative and increase in magnitude from the top of descent to the meter fix.

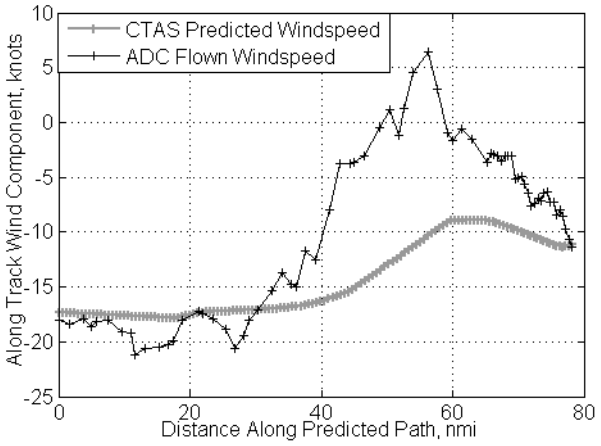

Figure 6. Example along track component of wind speed for run 34 showing a less of a headwind than was predicted.

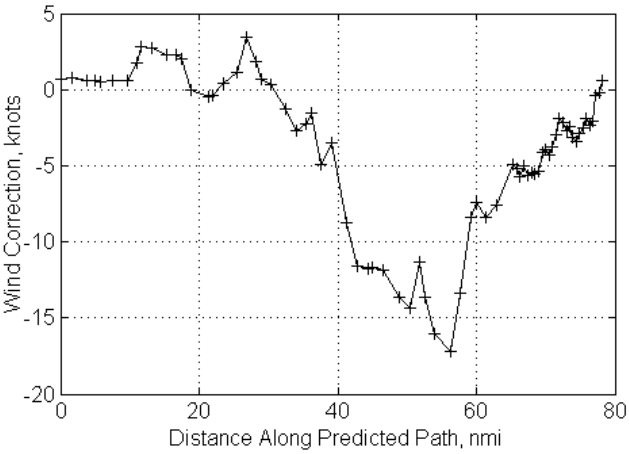

Figure 7. Example showing effect of corrected winds on groundspeed for run 34.

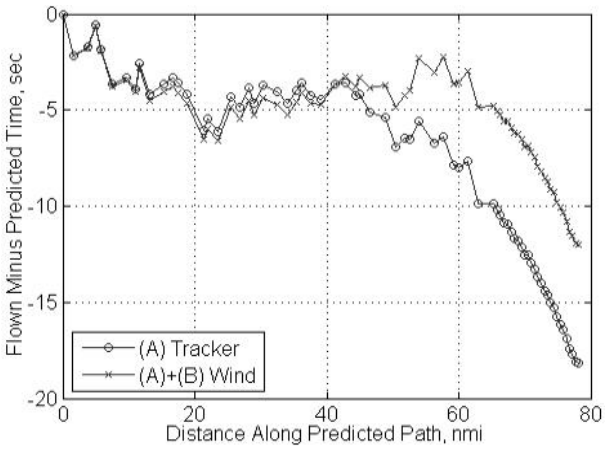

Figure 8. Example effect of wind on time error for run 34. Both curves have been corrected for tracker jumps. Curve with 'x' marker has also been corrected for wind.

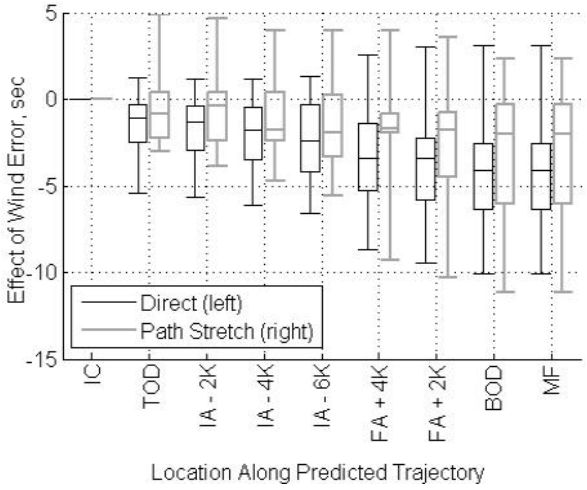

Figure 9. Wind error at locations along predicted trajectory.

C. CAS Deceleration

All aircraft were required to cross their assigned meter fix at or below a defined CAS. However, there may be differences in how the aircraft reduces CAS to meet the meter fix crossing airspeed. Generally, the Global 5000 aircraft did not level off at the meter fix altitude and reduce CAS in a level segment. The CTAS trajectory prediction was consistent with this behavior. However, the level-off segment was an error source for a few of the runs in which aircraft reached their bottom of descent before crossing the meter fix.

The start of the CAS deceleration segment was identified as the location where the aircraft is predicted to start reducing airspeed below the issued descent CAS. For example, in Fig. 10 the constant CAS of 300 knots was predicted to occur at approximately 53 to 60 nmi from the initial condition. While the aircraft was predicted to begin decelerating from 300 knots to 250 knots CAS starting at approximately 60 nmi from the initial condition. In this case, the aircraft actually maintained the descent CAS of 300 knots until approximately 70 nmi from the initial condition. At about 75 nmi along the predicted path the aircraft TAS is about 30 knots higher than was predicted as shown in the effect of CAS deceleration plot in Fig. 11. This difference would cause the aircraft to arrive at the meter fix 13 seconds earlier than predicted in the absence of other error sources as shown in the time error plot in Fig. 12.

The CAS deceleration error was aggregated to generate the box plot shown in Fig. 13. The deceleration error is negligible near the top of descent since only a few runs were predicted to begin the CAS deceleration segment within 6,000 ft of the initial altitude (IA-6K). The CAS deceleration error begins to grow significantly near the bottom of descent since this error correction is only applied in locations where the aircraft is predicted to be reducing CAS.

On average, the CAS deceleration errors are negative indicating a similar behavior to that shown in Fig. 10. The behavior in Fig. 10, and for the majority of the cases, has the predicted CAS deceleration starting to occur earlier than the flown trajectory and at a slower rate of deceleration. A faster flown deceleration rate allowed the aircraft to be closer to the meter fix before starting to decelerate

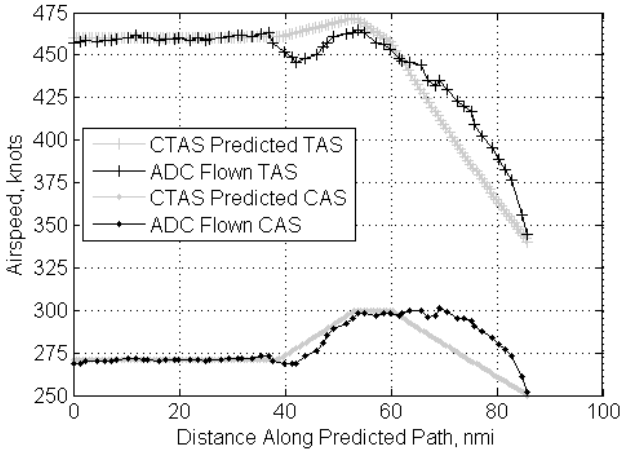

Figure 10. Example flown (ADC) and predicted (CTAS) TAS (top two curves) and CAS (bottom curves) for run 3 showing that the aircraft reduced CAS to 250 knots later than predicted.

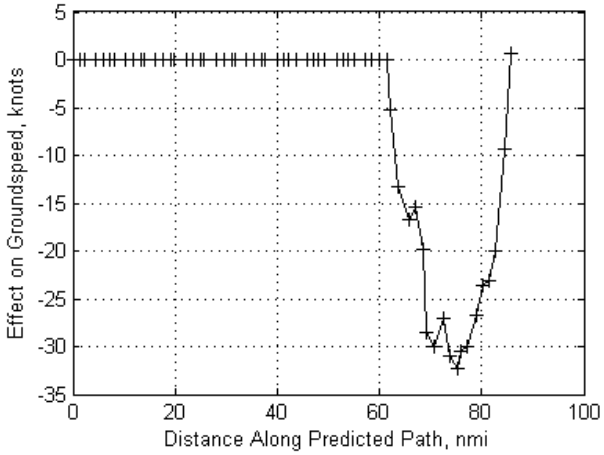

Figure 11. Example showing effect of corrected winds on groundspeed for run 3.

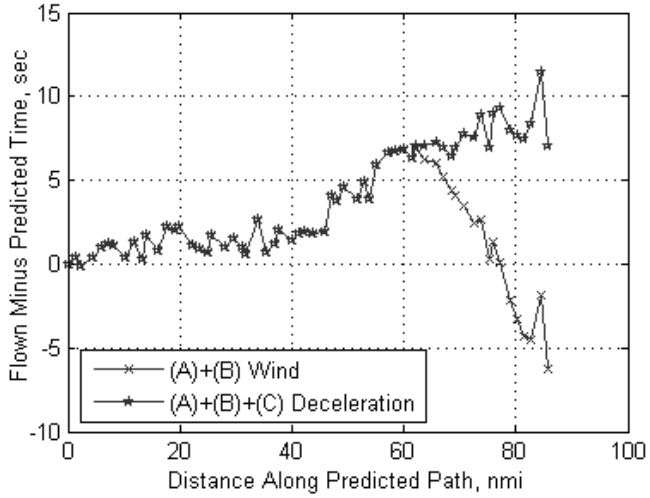

Figure 12. Example effect of CAS deceleration on time error for run 3. Both curves have been corrected for tracker jumps and wind. Curve with star marker has also been corrected for deceleration.

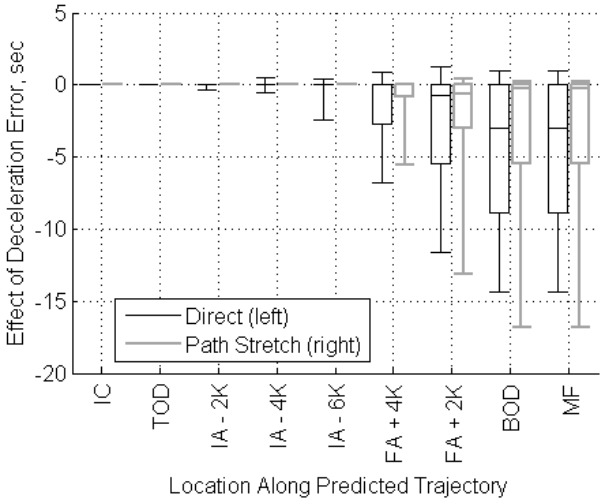

Figure 13. CAS deceleration error at locations along predicted trajectory.

D. Speed Conformance

A speed conformance error occurs when an aircraft deviates from its target CAS. For example, if an aircraft is targeting a descent CAS of 250 knots but is flying 260 knots then there is a speed conformance error of 10 knots.

This is the case for the example shown in Fig. 14, which is corrected starting at about 20 nmi from the initial condition (about 60 nmi from meter fix). The effect of corrected speed conformance on groundspeed is shown in Fig. 15. As the descent proceeds, the impact of speed conformance grows to about three seconds when the aircraft is at about 45 nmi from the initial condition. In the end, however, the impact of speed conformance correction does not have a significant impact on time error at the meter fix in this case, shown in Fig. 16.

The speed conformance groundspeed error source correction is applied along the predicted constant CAS segment between the predicted Mach to CAS transition location and the location where the aircraft is predicted to start to decelerate to meet the meter fix speed restriction. The start of the constant CAS segment was identified by two conditions: (1) the altitude is below the initial altitude and (2) the Mach is below the initial Mach for the en-route segment. The last data point of the segment is when the aircraft is predicted to start decelerating and the CAS drops below the descent CAS.

The speed conformance error was aggregated in order to generate the box plot shown in Fig. 17. Figure 17 shows that the effect of speed conformance grows between the top of descent and bottom of descent which in this study is expected since the correction is cumulative.

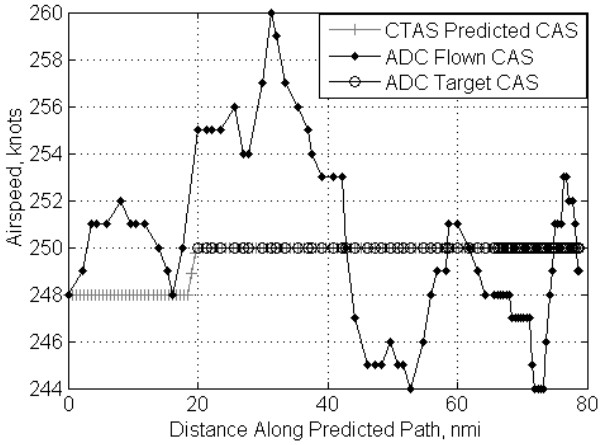

Figure 14. Example flown (ADC) and predicted (CTAS) CAS for run 43 showing deviation from 250 knot target CAS during descent.

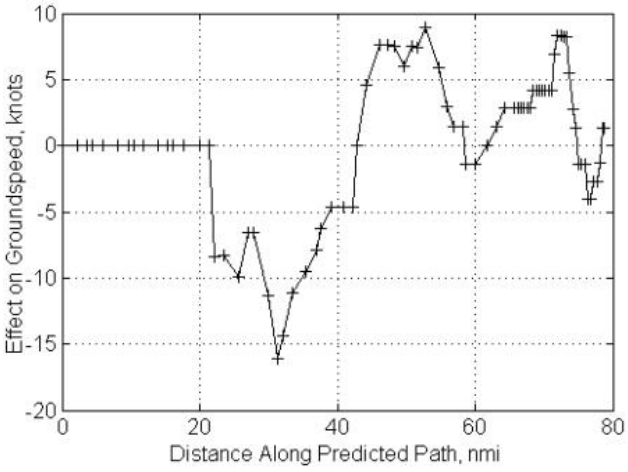

Figure 15. Example showing effect of corrected speed conformance on groundspeed for run 43.

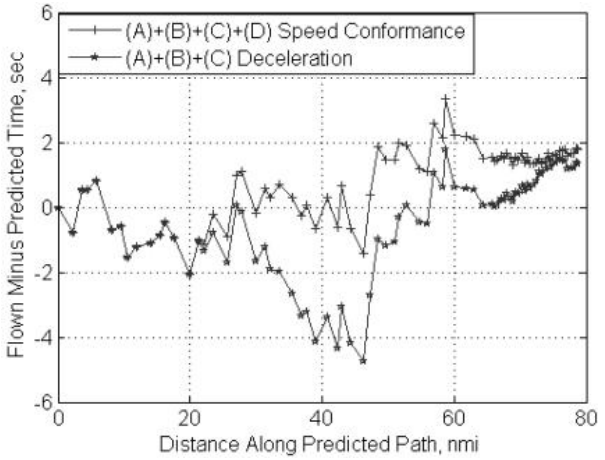

Figure 16. Example effect of speed conformance on time error for run 43. Both curves have been corrected for tracker jumps, wind, and deceleration. Curve with '+' marker has also been corrected for speed conformance.

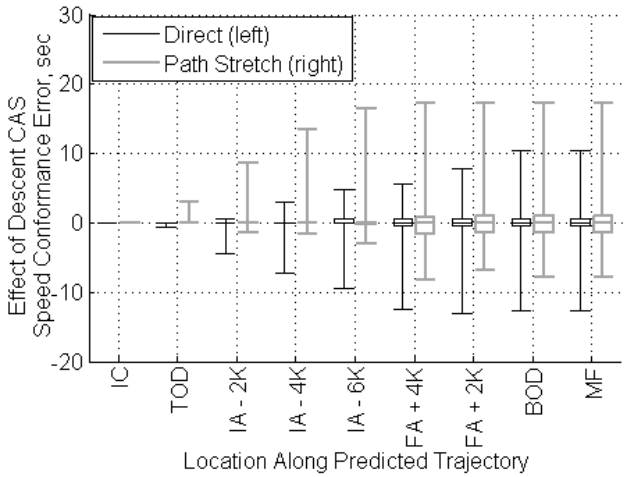

Figure 17. Speed conformance error at locations along predicted trajectory.

E. Target Mach

The aircraft may have been targeting a different Mach than was predicted by the CTAS trajectory synthesizer. Run 36 shown in Fig. 18 is an example of target Mach error where the aircraft is flying a faster Mach than predicted prior to the transition from constant Mach to constant CAS, located about 45 nmi downstream of the initial condition (about 35 nmi from the meter fix). The predicted Mach is low due to the low groundspeed estimated by the radar tracker after the aircraft turns onto the arrival route to begin its run. The flown target Mach of 0.76 (black 'o' marker), flown Mach between 0.73 and 0.76 (black diamond marker), and predicted Mach of 0.72 (grey '+' marker) are all shown in Fig. 18. This Mach difference is converted into an effect on groundspeed as shown in Fig. 19. Applying this groundspeed correction in Fig. 20 shows that the faster Mach causes the aircraft to arrive to the meter fix about 15 seconds earlier than predicted.

The target Mach error was aggregated in order to generate the box plot shown in Fig. 21. Figure 21 shows that, on average, the aircraft flew a faster Mach than was predicted (negative values). Also, as expected, the target Mach error primarily occurred prior to top of descent since during descent the aircraft transitions to constant CAS. The target Mach error was higher for path stretch runs than direct runs since the initial condition for path stretch runs is closer to the turn from the repositioning route to the arrival route (i.e., further from the meter fix) which causes the path stretch runs to be impacted more by the groundspeed estimated by the radar tracker than the direct runs.

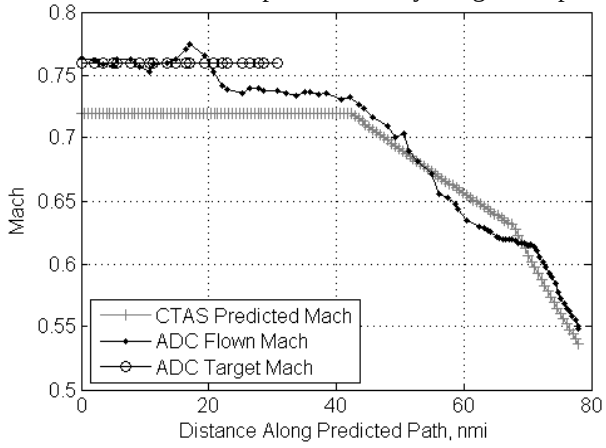

Figure 18. Example flown (ADC) and predicted (CTAS) Mach for run 36 showing deviation from the 0.72 target Mach prior to the constant Mach to constant CAS transition.

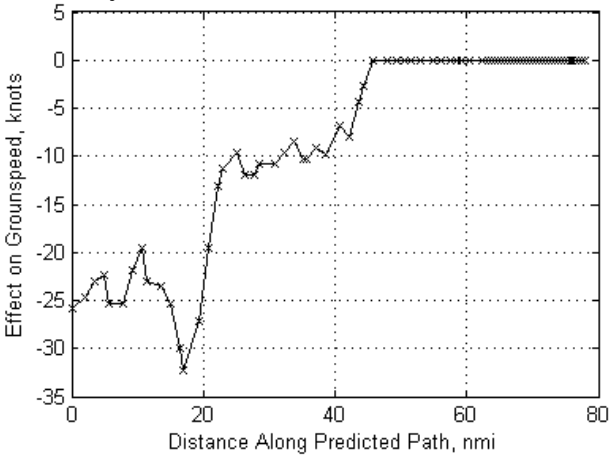

Figure 19. Example showing effect of corrected target Mach on groundspeed for run 36.

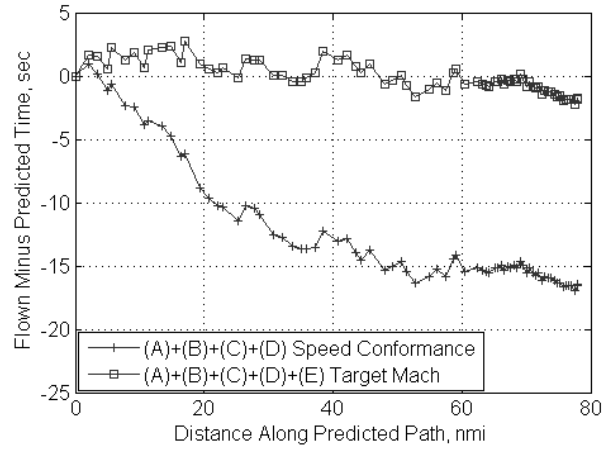

Figure 20. Example effect of a different Mach than predicted on time error for run 36. Both curves have been corrected for tracker jumps, wind, deceleration, and speed conformance. Curve with square marker has also been corrected for target Mach.

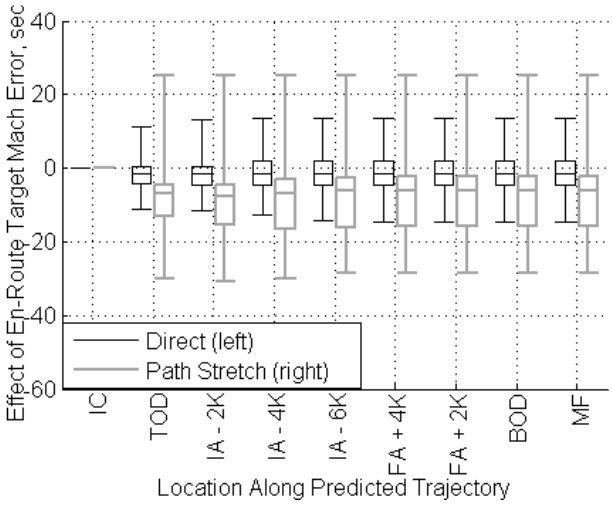

Figure 21. Target Mach error at locations along predicted trajectory.

F. Atmosphere / Altitude

Atmospheric conditions including temperature and air density are used to convert the targeted airspeed to TAS which, taking into account winds, is then converted to groundspeed. This error source focused on the predicted vs. flown atmospheric conditions which introduce errors in the conversion of Mach and CAS to TAS. In the case of Mach, TAS is the product of Mach, speed of sound at sea level (a constant), and the square root of the ratio of static air temperature in which the aircraft is flying (recorded by ADC) to the temperature at sea level (a constant). In the case of CAS, TAS is a product of CAS and the square root of the ratio of air density at sea level (a constant) to the air density in which the aircraft is flying (recorded by ADC). Flying higher or lower than predicted similarly changes the TAS and was also captured by this error source.

For example, Fig. 22 shows a case where the aircraft was up to 175 ft lower than predicted from the top of descent at about 20 nmi from the initial condition to about 15 nmi from the meter fix. This caused the aircraft to be flying about 1 to 1.5 knots faster than predicted which is corrected according to the effect of atmosphere / altitude on groundspeed plot in Fig. 23. Fig. 24 shows that the atmosphere and altitude correction increased the arrival time error from about one second to about two seconds.

The box plot aggregating the atmosphere and altitude errors in Fig. 25 shows that the error primarily impacts the descent portion which is expected since this is the location most likely to have a difference between predicted and flown altitudes. The negative medians in the box plot indicate that, on average, the aircraft flew a lower altitude than predicted which increased groundspeed and caused the aircraft to arrive at the meter fix earlier than predicted.

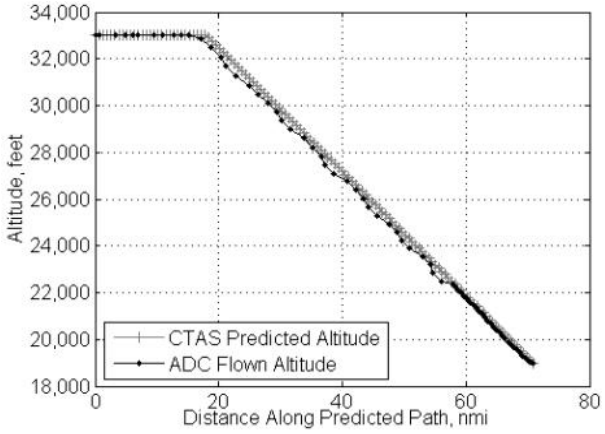

Figure 22. Example predicted and flown altitude for run 14.

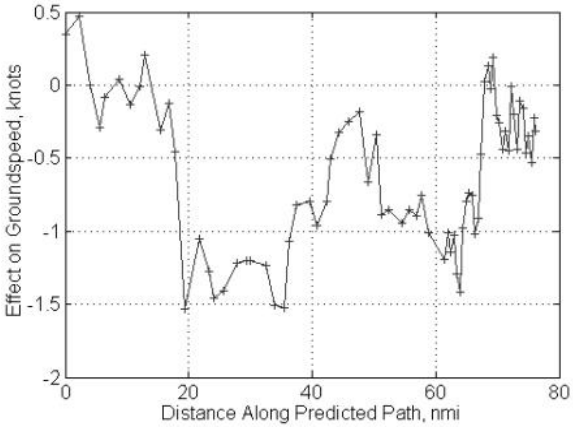

Figure 23. Example showing effect of corrected atmosphere/altitude on groundspeed for run 14.

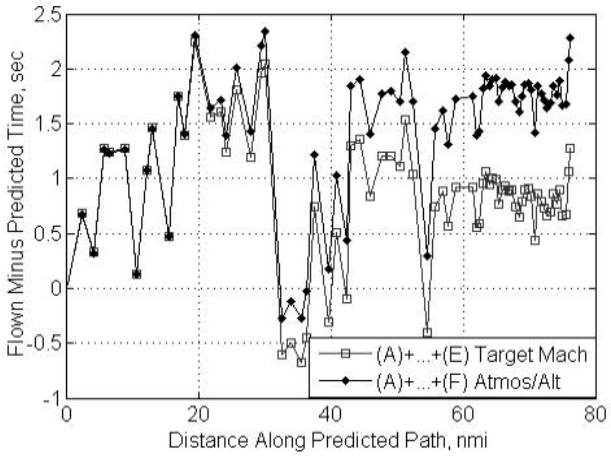

Figure 24. Effect of atmosphere and altitude on time error for run 14. Curve with diamond marker has been corrected for atmosphere and altitude.

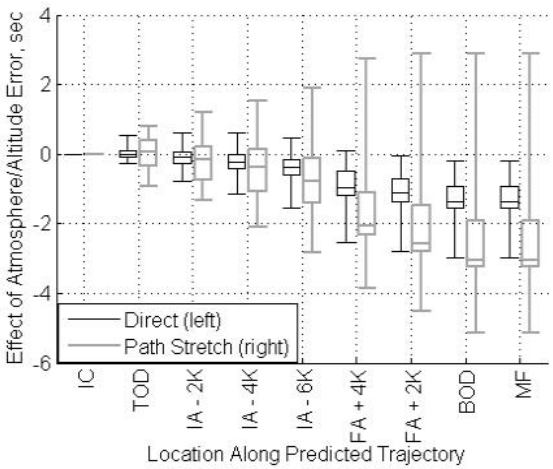

Figure 25. Atmosphere and altitude error at locations along predicted trajectory.

G. Path Distance

Aircraft deviated from their predicted lateral path causing variance in the distance from the initial condition to the meter fix. For direct runs, any variance from the predicted lateral path would result in a longer flown path distance than predicted. However, all of the path stretch runs flew a shorter path through the turn than predicted. The lateral profile in Fig. 26 is an example of using a shorter path midway through a southeast-bound descent that starts in the upper right of the plot. At the middle of the curve the aircraft is about 1.8 nmi away from the predicted lateral path (i.e., cross-track error of 1.8 nmi). This path is about 1.2 nmi shorter than predicted and is applied as a change in path distance shown in Fig. 27 rather than the groundspeed change applied in the previous error sources excluding tracker jumps. The shorter path distance contributes about nine seconds to the aircraft being early to the meter fix as shown in the time error plot in Fig. 28. As expected the shorter path distance in the path stretch runs caused the aircraft to arrive earlier than predicted as shown in the box plot that aggregates the path distance in Fig. 29. The path stretch occurs at or near the top of descent which is why the effect of path distance is primarily before the top of descent as shown in Fig. 29. The longer path distance in the direct runs caused the aircraft to arrive later than predicted as indicated by the positive errors in Fig. 29.

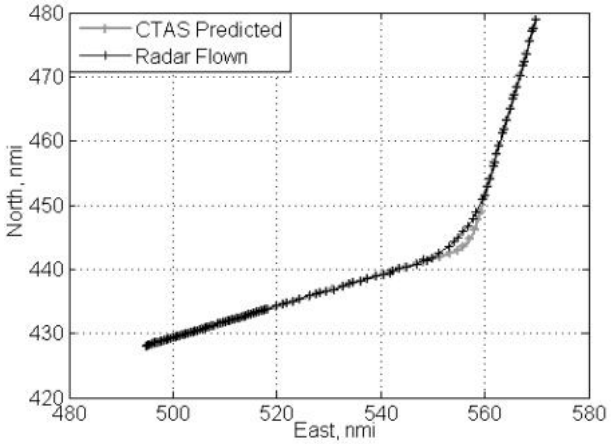

Figure 26. Example predicted and flown lateral path for run 33.

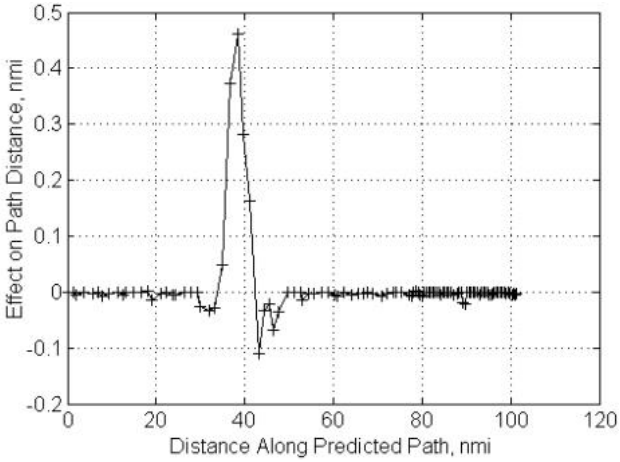

Figure 27. Example showing effect of path distance correction for run 33.

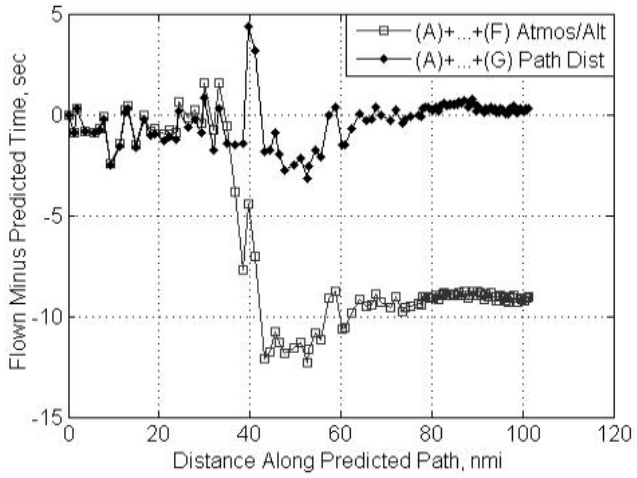

Figure 28. Example effect of path distance on time error for run 33. Curve with diamond marker has been corrected for path distance.

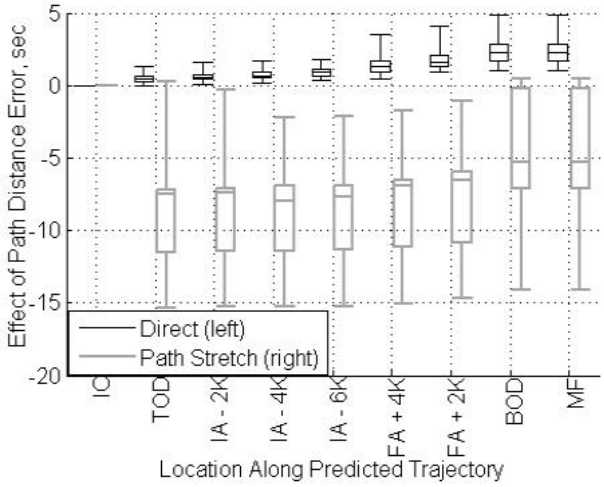

Figure 29. Path distance error at locations along predicted trajectory.

V. Results

This section presents the combined impact of the seven trajectory prediction error sources at locations along the predicted trajectory. Also, the percentage contribution of the error sources to the total time error variance at the meter fix is shown. A comparison to the results of a 1994 flight test using NASA's Boeing 737 test aircraft is presented last.

A. Magnitude of Error Sources

The magnitude of the error sources are shown at the top of descent (Fig. 30) and meter fix (Fig. 31). In both of the figures the seven error sources from tracker jumps (error source A) to path distance (error source G) are presented along the x-axis. Also presented on the x-axis are the combined effect of these seven error sources (total error) and the residual error after correcting for these seven error sources. Figure 30 shows the contribution of each error source to time errors that accumulate from the initial condition to the top of descent. Comparing Fig. 31 to Fig. 30 shows the contribution of each error source that accumulate during descent from the top of descent to the meter fix.

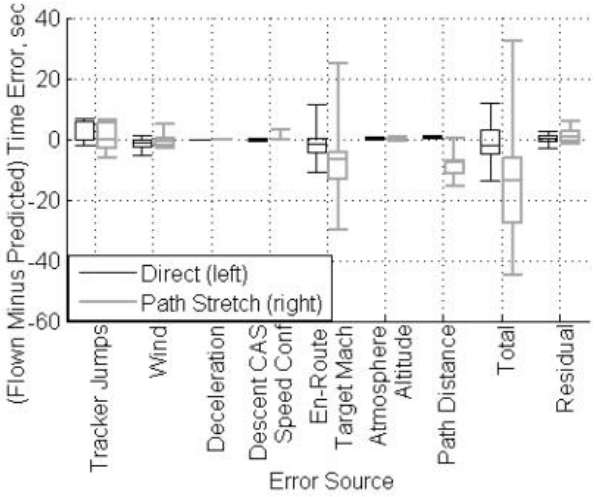

Figure 30. Relative magnitude of the error sources and residual error at top of descent.

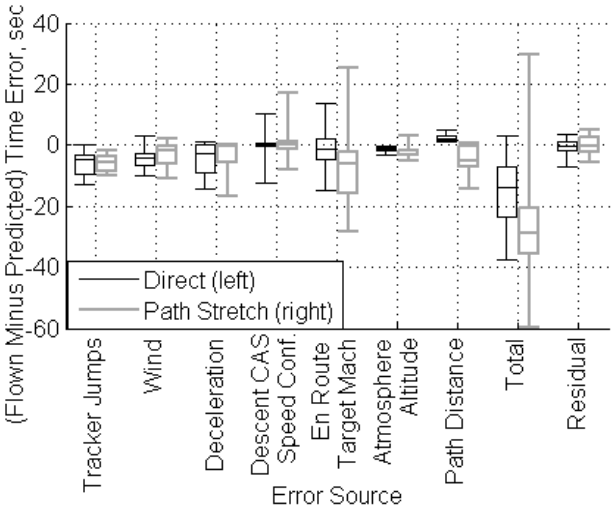

Figure 31. Relative magnitude of the error sources and residual error at meter fix.

For direct runs the target Mach error source is the most dominant error source at the top of descent (μ=-1.7 sec, σ=4.3 sec at TOD) and remains, relatively, the most significant error source throughout the descent (μ=-1.1 sec, σ=5.7 sec at MF) as measured by the standard deviation of the error sources. The focus is more on the standard deviation of the error rather than the mean of the error since the mean and median effects of the error sources are generally close to zero but there can be a large spread in the data. The deceleration error source becomes significant (μ=-5.0 sec, σ=5.2 sec at MF), and approximately the same magnitude of effect as target Mach near the meter fix. The wind, speed conformance, altitude / atmosphere, and path distance error sources are the smallest in magnitude relative to the other error sources at the meter fix.

For path stretch runs the target Mach error source has the largest effect on time error throughout the descent. As expected, the path stretch results in higher contributions of path distance to total error for the path stretch runs (μ=-5.2 sec, σ=5.0 sec at MF) as compared to the direct runs (μ=2.3 sec, σ=0.9 sec at MF). The other error sources have a similar and less significant effect on the total error than target Mach and path distance.

A summary of the mean and standard deviation of the effect of the error sources at the meter fix is included in Table 3. For example, the row for en-route target Mach shows a -1.1 and 5.7 second mean and standard deviation respectively for direct descents and a -7.5 and 15.9 second mean and standard deviation respectively for path stretch descents. The difference between the direct and path stretch runs may be attributed to the path stretch routing which was in close proximity of a turn. Mean and standard deviation at six locations along the predicted trajectory are included in Table 6 in the Appendix for completeness.

B. Percentage Contribution to Total Variance

The contributions of each error source to the mean total error at the meter fix are a straightforward summation of the mean errors. However, the percentage contribution of each error source to the variance (σ^2) of the time error at the meter fix requires estimating and applying a variance-covariance matrix shown in rows labeled "cov" in Tables 4 and 5 for direct and path stretch runs respectively.

Table 3. Mean (μ) and standard deviation (σ) at the meter fix for 2010 Global 5000 error sources and equivalent 1994 Boeing 737 test aircraft error sources. Mean and standard deviation in units of seconds.

2010 Global 5000 Flight Trial					1994 B737 Test Aircraft Flight Trial		
Error Source	Direct		Path Stretch		Equivalent Error Source	Turn*	
	μ	σ	μ	σ		μ	σ
A. Tracker Jumps	-6.1	3.7	-6.0	2.9	*Corrected before error analysis*		
B. Wind	-4.0	3.4	-3.1	4.5	Wind	-5.0	11.0
C. CAS Deceleration	-5.0	5.2	-3.5	5.6	*See airspeed conformance below*		
D. Speed Conformance	0.1	3.4	1.0	6.7			
C+D. Decel. + Speed Conf.	-4.9	6.1	-2.5	3.1	Airspeed conformance	-1.0	2.4
E. En-Route Target Mach	-1.1	5.7	-7.5	15.9	Initial groundspeed	-1.6	1.5
F. Atmosphere / Altitude	-1.3	0.6	-2.3	2.3	Temperature	1.3	1.1
					Altitude	1.6	2.4
G. Path Distance	2.3	0.9	-5.2	5.0	Turn overshoot	-0.3	0.7
Total	-15.6	9.9	-27.0	25.8	Total†	-4.6	13.9
Residual	-0.6	2.5	-0.4	3.4	Residual	2.6	1.6

The diagonal of the variance-covariance matrix is the variance for each of the error sources. For example, the variance of the tracker jumps error source at the meter fix (σ^2 = 13.5 sec^2) shown in the upper left in Table 4 is the square of the standard deviation at the meter fix (σ = 3.7 sec) shown in Table 3. The covariance values off the diagonal can be either positive or negative. Positive covariance indicates a relationship where higher values of one error source are associated with higher values of another error source. For example, for the covariance in Table 4 for direct runs, the covariance between wind and speed conformance (σ^2 = 2.42 sec^2) is positive indicating that higher time errors caused by wind are associated with higher time errors caused by speed conformance.

Negative covariance indicates a relationship where higher values of one error source are associated with lower values of another compensating error source. For example, for the covariance in Table 5 for path stretch runs, the covariance between deceleration and speed conformance (σ^2 = -32.79 sec^2) is negative indicating that higher speed conformance errors are associated with lower deceleration errors. A normalized correlation coefficient that ranges from -1 to 1 is also shown in Tables 4 and 5 to show the strength of a linear relationship between the error sources.

The total variance is the sum of all elements in the variance-covariance matrices in Tables 4 and 5 for direct ($\sigma^2 = 9.88^2$ = 97.54 sec^2) and path stretch runs ($\sigma^2 = 25.78^2$ = 664.73 sec^2) respectively. It is not possible to completely decouple the error sources due to the contribution of the covariance to the total variance. However, a rough estimate is made based on assigning half of the covariance to each of the two error sources. For example, the covariance between tracker jumps and wind is -3.02 sec^2 which appears twice in the covariance matrix since the matrix is symmetrical for a contribution of -6.04 sec^2 to the total variance. Therefore, the -3.02 sec^2 covariance is assigned to both tracker jumps and wind error sources. The variance and half the covariance is then added for each error source and divided by the total variance (i.e., sum the columns in Tables 4 and 5 and divide by the total variance).

The target Mach error source (30.6% for direct and 60.2% for path stretch) had the highest contribution to the total time error variance at the meter fix. The target Mach error source for direct runs also had significant positive covariance with the other error sources which resulted in a higher contribution to the total time error variance than would have occurred in the absence of other error sources. Deceleration (23.7% for direct and -17.5% for path stretch) and speed conformance (14.0% for direct and 16.8% for path stretch) are other error sources with a relatively large contribution to the total time error variance.

C. Comparison to 1994 Flight Test using NASA's Boeing 737 Test Aircraft

An analysis on trajectory error sources was performed for a NASA B737 test aircraft using results from a 1994 EDA field trial.[10] Results were compared with the results based on the 2010 flight trial using Global 5000 aircraft.

* The turn in 1994 was similar to the path stretch runs in 2010 in that the waypoint defining the turn was programmed into the FMS prior to descent.

† Excludes experimental error source.

The earlier study considered four levels of cockpit automation. The comparison presented here will focus on the 1994 runs based on a conventional FMS with LNAV and VNAV. Seven error sources were identified in the earlier field trial: (1) experimental error, (2) temperature, (3) airspeed conformance, (4) altitude, (5) initial ground-speed, (6) turn overshoot, and (7) wind. The mean and standard deviation of these error sources are shown in the right of Table 3.

The total error was lower in 1994 (μ=-4.6 sec, σ=13.9 sec) than the error in 2010 for direct (μ=-15.6 sec, σ=9.9 sec) and path stretch runs (μ=-27.0 sec, σ=25.8 sec). However, the experimental setup in 1994 was different than 2010 which complicates the comparison. There was a position bias in the radar tracker in 1994 which lead to the error source analysis being partly based on GPS position data recorded onboard the B737 rather than using the radar tracker position (radar tracker speed was still used for the initial condition). Therefore, the tracker jump error source in 2010 has no equivalent in 1994. The 1994 initial condition was based on both cruise and descent speeds issued by controllers which reduces the error in estimated Mach at the initial condition. In 2010 only the issued descent speed was used in generating CTAS predictions and the target Mach was estimated by the radar tracker groundspeed, rather than by the Mach issued by ATC, which increases this error source relative to 1994. Lastly, the 1994 flight trial used a calibrated B737 model in CTAS that would better predict turns than the 2010 Global 5000 turn model.

Table 4. Variance-Covariance (cov) and correlation (corr) matrix among error sources for direct run arrival time errors to the meter fix. Covariance is in units of sec^2 and correlation is dimensionless.

	Covariance (cov) Correlation (corr)	A. Tracker Jumps	B. Wind	C. CAS Deceleration	D. Speed Conformance	E. En-Route Target Mach	F. Atmosphere / Altitude	G. Path Distance	Residual
A. Tracker Jumps	cov	13.49	-3.02	-1.26	-1.77	1.58	0.67	-0.88	0.02
	corr	*1.00*	*-0.24*	*-0.07*	*-0.14*	*0.07*	*0.29*	*-0.27*	*0.00*
B. Wind	cov	-3.02	11.52	3.49	2.42	-4.47	-0.28	1.26	-1.40
	corr	*-0.24*	*1.00*	*0.20*	*0.21*	*-0.23*	*-0.13*	*0.42*	*-0.17*
C. CAS Deceleration	cov	-1.26	3.49	27.26	-0.45	-6.25	-1.00	1.68	-0.35
	corr	*-0.07*	*0.20*	*1.00*	*-0.03*	*-0.21*	*-0.30*	*0.37*	*-0.03*
D. Speed Conformance	cov	-1.77	2.42	-0.45	11.30	0.74	-0.02	0.69	0.75
	corr	*-0.14*	*0.21*	*-0.03*	*1.00*	*0.04*	*-0.01*	*0.23*	*0.09*
E. En-Route Target Mach	cov	1.58	-4.47	-6.25	0.74	32.99	2.54	-0.45	3.19
	corr	*0.07*	*-0.23*	*-0.21*	*0.04*	*1.00*	*0.70*	*-0.09*	*0.22*
F. Atmosphere / Altitude	cov	0.67	-0.28	-1.00	-0.02	2.54	0.40	-0.05	0.08
	corr	*0.29*	*-0.13*	*-0.30*	*-0.01*	*0.70*	*1.00*	*-0.10*	*0.05*
G. Path Distance	cov	-0.88	1.26	1.68	0.69	-0.45	-0.05	0.78	-0.64
	corr	*-0.27*	*0.42*	*0.37*	*0.23*	*-0.09*	*-0.10*	*1.00*	*-0.29*
Residual	cov	0.02	-1.40	-0.35	0.75	3.19	0.08	-0.64	6.18
	corr	*0.00*	*-0.17*	*-0.03*	*0.09*	*0.22*	*0.05*	*-0.29*	*1.00*
Sum of covariance		8.83	9.52	23.12	13.66	29.87	2.34	2.39	7.83
% of total variance		*9.1%*	*9.8%*	*23.7%*	*14.0%*	*30.6%*	*2.4%*	*2.4%*	*8.0%*

Table 5. Variance-Covariance (cov) and correlation (corr) matrix among error sources for path stretch run arrival time errors to the meter fix. Covariance is in units of sec^2 and correlation is dimensionless.

	Covariance (cov) Correlation (corr)	A. Tracker Jumps	B. Wind	C. CAS Deceleration	D. Speed Conformance	E. En-Route Target Mach	F. Atmosphere / Altitude	G. Path Distance	Residual
A. Tracker Jumps	cov	8.57	-4.06	-1.76	-2.40	23.02	2.14	5.44	7.68
	corr	*1.00*	*-0.30*	*-0.11*	*-0.12*	*0.49*	*0.32*	*0.37*	*0.77*
B. Wind	cov	-4.06	20.68	-13.30	16.07	-6.81	1.01	-4.46	-1.30
	corr	*-0.30*	*1.00*	*-0.53*	*0.53*	*-0.09*	*0.10*	*-0.20*	*-0.08*
C. CAS Deceleration	cov	-1.76	-13.30	30.99	-32.79	-63.80	-10.38	-15.35	-10.01
	corr	*-0.11*	*-0.53*	*1.00*	*-0.88*	*-0.72*	*-0.82*	*-0.55*	*-0.53*
D. Speed Conformance	cov	-2.40	16.07	-32.79	44.48	57.71	10.74	10.31	7.36
	corr	*-0.12*	*0.53*	*-0.88*	*1.00*	*0.54*	*0.71*	*0.31*	*0.32*
E. En-Route Target Mach	cov	23.02	-6.81	-63.80	57.71	253.96	33.49	59.00	43.69
	corr	*0.49*	*-0.09*	*-0.72*	*0.54*	*1.00*	*0.92*	*0.74*	*0.80*
F. Atmosphere / Altitude	cov	2.14	1.01	-10.38	10.74	33.49	5.17	6.72	4.97
	corr	*0.32*	*0.10*	*-0.82*	*0.71*	*0.92*	*1.00*	*0.59*	*0.64*
G. Path Distance	cov	5.44	-4.46	-15.35	10.31	59.00	6.72	24.89	9.26
	corr	*0.37*	*-0.20*	*-0.55*	*0.31*	*0.74*	*0.59*	*1.00*	*0.54*
Residual	cov	7.68	-1.30	-10.01	7.36	43.69	4.97	9.26	11.65
	corr	*0.77*	*-0.08*	*-0.53*	*0.32*	*0.80*	*0.64*	*0.54*	*1.00*
Sum of covariance		38.63	7.83	-116.40	111.48	400.26	53.86	95.81	73.30
% of total variance		*5.8%*	*1.2%*	*-17.5%*	*16.8%*	*60.2%*	*8.1%*	*14.4%*	*11.0%*

For these reasons a comparison of the total error between 1994 and 2010 was made based on mean of the following error sources: wind, CAS deceleration, airspeed conformance, atmosphere, altitude, and temperature. When comparing this error source subset the total mean error is higher in 2010 for both direct (μ=-10.2 sec) and path stretch (μ=-7.9 sec) runs than occurred in 1994 (μ=-3.4sec). This higher error is primarily due to higher CAS deceleration errors in 2010. A discussion of the seven 1994 error sources is included next with their closest equivalent error source identified in 2010.

Experimental errors were caused by CTAS computational and data errors that were corrected after the 1994 flight trial. These errors did not exist in the results from the Global 5000 runs.

Temperature and altitude were combined into a single error source with a resulting mean and standard deviation less than three seconds for both direct and path stretch runs. The 1994 results were similar, with temperature having a negligible effect and altitude have a small effect.

The 1994 airspeed conformance error contributed one second to the arrival time error (μ = 1.0 sec, σ = 2.4 sec). The 2010 Global 5000 runs had higher standard deviation of the errors associated with speed conformance for both the direct (μ=0.1 sec, σ=3.4 sec) and path stretch (μ=1.0 sec, σ=6.7 sec) runs. CAS deceleration was quantified separately from speed conformance for the 2010 Global 5000 runs but not for the 1994 results. Speed conformance and CAS deceleration can be combined using variance and covariance to derive a standard deviation of 6.1 seconds for direct cases and 3.1 seconds for path stretch cases. Both are larger than the 1994 airspeed conformance standard

deviation of about 2 seconds. The different airspeed conformance and deceleration errors between 1994 and 2010 are potentially due to different aircraft and different flight crews. The different errors due to airspeed conformance could also be attributed to VNAV being guidance only and not coupled to the autopilot or autothrottle. The 1994 test non-FMS runs exhibited a four second standard deviation of airspeed conformance errors which is higher than the about two second standard deviation exhibited by the test aircraft that used the FMS with LNAV and VNAV capabilities. For this reason the 2010 airspeed conformance standard deviation of 3.4 seconds is consistent with expectations that it would fall between the standard deviation for non-FMS runs and runs with LNAV and VNAV.

The different errors due to deceleration, in addition to different aircraft types and flight crew, could be caused by the procedure to meet the meter fix crossing speed. In 1994 the aircraft CAS was reduced by maintaining idle thrust at bottom of descent, pitching the aircraft to a level segment, and then using the level segment to reduce speed to meet the meter fix crossing speed. In 2010 the descent CAS was reduced by reducing throttle to at or near idle, using pitch to maintain the vertical profile, and using speed brakes as needed to meet the meter fix crossing speed restriction. It is easier to predict a reduction in CAS during a level segment rather than in descent since the level segment deceleration procedure is more standardized.

The en-route target Mach error source has roughly the same cause as the initial ground-speed used in the error source analysis of the 1994 field trial. However, the 2010 Global 5000 runs had much higher errors attributed to the target Mach for direct (μ=-1.1 sec, σ=5.7 sec) and path stretch (μ=-7.5 sec, σ=15.9 sec) runs as compared to the error source analysis of initial groundspeed (μ =-1.6 sec, σ=1.5 sec) from the 1994 trial. The higher target Mach error in 2010 is attributed in large part to the aircraft turning onto the arrival route closer (about 90 to 120 nmi from meter fix) to the meter fix than in 1994 (about 130 nmi from meter fix). This turn causes a transient error in the radar track groundspeed estimate, often lower than the aircraft's actual, at the initial condition. A lower groundspeed, from which Mach is determined by subtracting out winds and converting TAS to Mach using atmospheric conditions, results in a lower Mach than was recorded on the aircraft.

The turn overshoot (μ=0.3 sec, σ=0.7 sec) is roughly equivalent to the path distance (μ=-5.2 sec, σ=5.0 sec) error source. However, in the 2010 Global 5000 path stretch runs, the aircraft consistently undershot the turn causing the aircraft to arrive earlier than predicted at the meter fix and resulted in a larger standard deviation than was observed in 1994. Potential reasons for the difference are as follows. The turn radius of an aircraft is defined by groundspeed and bank angle. A higher groundspeed requires a longer turn radius at the same bank angle. The flown groundspeed is higher than predicted (discussed in the previous paragraph) which is consistent with a larger flown turn radius as compared to the CTAS predicted turn radius. Another possibility is that the bank angle used by CTAS in 1994 was more appropriate for a Boeing 737 than the bank angle used by CTAS in 2010 for a Global 5000 aircraft.

Winds aloft prediction had a larger effect on the standard deviation of meter fix arrival time error in 1994 (μ=-5 sec, σ=11 sec) than in 2010 for both the direct (μ=-4.0 sec, σ=3.4 sec) and path stretch (μ=-3.1 sec, σ=4.5 sec) cases. The predicted wind speed error often exceeded 20 knots, and exceeded 60 knots in some cases, in 1994. By comparison, only four of the 44 runs had wind speed errors that exceeded 15 knots, and none of the runs experienced a greater than 20 knot wind speed error at any location along the trajectory. These lower wind speed errors were a result of better winds aloft predictions in 2010 that are more appropriate for trajectory prediction than the wind models used in 1994. For example, CTAS wind updates in 2010 occurred at a one-hour interval, which is more frequent than the three-hour interval used in 1994. Besides the reduction of the RUC wind forecast interval from three hours (available in 1994) to one hour (available in 2010), improvements in the state of the art have reduced wind forecast errors substantially[18].

D. Comparison to 2009 3D PAM Flight Trial using Revenue Flights

A 3D PAM field trial was conducted at Denver in September 2009 using Boeing 737, Boeing 757, and Airbus 319/320 aircraft during revenue flights[3]. Analysis was performed on 270 flights issued cruise and descent speeds that were uninterrupted during descent. The TOD error and meter fix arrival time error were calculated differently for the 2009 flight trial than for the 2010 flight trial. However, an approximate comparison is presented next. The direct runs were used for comparison since they were less influenced by the turn near the initial condition. This turn would generally not exist in the revenue flights.

The TOD prediction error in 2009 was reported as a mean absolute value of 5.4 nmi with 47% of the flights with less than 5 nmi error. The TOD prediction error in 2010 was an order of magnitude smaller at 0.7 nmi mean absolute value with 100% of the runs with less than 5 nmi error.

The arrival time error in 2009 was reported as 11.5 seconds mean absolute value with 80% of the flights having an error less than 20 seconds. The error in 2010 was 15.6 seconds mean absolute value with 67% of the runs having an arrival time error less than 20 seconds. However, if the deceleration error source was removed, as would be expected if the Global 5000 decelerated in a more predictable level segment, the error would be reduced to 11.2

seconds mean absolute value with 83% of the runs having an arrival time error less than 20 seconds. The Global 5000 results in 2010 are similar to the Boeing and Airbus results of 2009 in the absence of a Global 5000 deceleration prediction error. To definitively confirm this result the Global 5000 runs would need to be repeated using the different deceleration procedure.

E. Error Mitigation

Several of the error sources identified in 2010 lend themselves to significant improvement with modest to no changes to ATC automation and/or procedures. The tracker jump error source may require no additional mitigation strategy because the FAA En Route Automation Modernization (ERAM) was deployed after the 2010 flight trial. ERAM replaces the En Route Host tracker with a more modern algorithm that is expected to greatly reduce, if not eliminate, the radar track jumps.

The CAS deceleration error source could be reduced by using a level segment deceleration similar to the procedure used by large jets. This level segment CAS deceleration is expected to be more predictable than deceleration during descent.

There are multiple changes that could reduce the magnitude of the en route target Mach error source. The ERAM radar tracker is expected to more accurately estimate groundspeed during turns and therefore reduce the magnitude of the en route target Mach error source. The impact of the turn could also be mitigated by limiting trajectory prediction updates to more steady state conditions which is more closely aligned with 3D PAM validation tests. Another target Mach mitigation strategy could be to use both the issued cruise airspeed and descent speed for trajectory predictions. This flight trial was based on passively estimating airspeed at the initial condition using radar track groundspeed, which is converted to airspeed by considering winds and atmosphere. This more closely represents the conditions of an en-route conflict probe. However, it would be more consistent with existing 3D PAM validation testing to have ATC issue cruise airspeed and use the airspeed for the trajectory prediction.

The path distance error source is influenced by the turn modeling in CTAS. Path distance errors could be reduced by calibrating an aircraft model that is used in CTAS to better predict aircraft behavior during turns.

VI. Conclusions

This paper estimated the trajectory prediction accuracy and error sources of 3D PAM descents based on a field trial at Denver International Airport using the Global 5000 aircraft. The predicted trajectory used the CTAS trajectory synthesizer and data known on the ground prior to the aircraft descending approximately 60 to 120 nmi from the meter fix. The flown trajectory and other data, including atmospheric and wind conditions, were obtained from an onboard air data computer. The Global 5000 aircraft arrived to the meter fix about 15 and 27 seconds earlier than predicted on average for direct and path stretch runs respectively. There was observed to be about a 10-second (direct) and 26-second (path stretch) standard deviation of the error associated with the early arrival of the Global 5000 aircraft.

Seven error sources were identified including (a) tracker jumps, (b) wind, (c) deceleration to fix crossing speed, (d) speed conformance during descent, (e) targeted Mach prior to descent, (f) atmosphere and altitude, and (g) path distance. Targeted Mach had the largest effect on arrival time error variance representing about 31% (direct) and 60% (path stretch) of the total arrival time error variance. The target Mach error was due to radar track groundspeed errors associated with maneuvers to reposition the aircraft to initiate each run. Speed conformance representing 14% (direct) and 17% (path stretch) as well as CAS deceleration representing 24% (direct) and -18% (path stretch) are the next highest components of total variance. Four of the error sources, tracker jumps, CAS deceleration, target Mach, and path distance, lend themselves to significant improvement with modest to no changes to ATC automation and/or procedures. These changes could significant reduce trajectory prediction error.

The TOD prediction error in 2010 was an order of magnitude smaller than in 2009. While the mean arrival time error was about 30% higher in 2010 compared to 2009, if the deceleration error source was removed as it would be if the Global 5000 decelerated in a level segment then the results would be on par. When comparing the 2010 results to the 1994 results the largest difference not due to experimental design and artifact was the impact of the wind prediction error. The reduction from 11-second standard deviation in 1994 to a less than 5-second standard deviation in 2010 was in large part due to better winds aloft prediction.

Appendix

This appendix presents more extensive numerical results than was included in the main body of the paper. The mean (μ) and standard deviation (σ) of the effect of the seven error sources at six locations between top of descent and the meter fix inclusive are shown in Table 6 for both direct runs (labeled as the “D” rows) and path stretch runs (label as the “PS” rows).

Table 6. Mean (μ) and standard deviation (σ) of error sources at locations along predicted trajectory for both direct runs (D) and path stretch runs (PS).

Error Source	D or PS	TOD		IA-4K		IA-6K		FA+4K		FA+2K		MF	
		μ	σ	μ	σ	μ	σ	μ	σ	μ	σ	μ	σ
A. Tracker Jumps	D	1.66	3.01	-0.67	4.04	-1.43	4.32	-2.51	5.79	-5.82	4.18	-6.08	3.67
	PS	0.38	4.92	-0.03	4.77	-2.36	4.56	-5.69	3.35	-6.03	2.93	-6.03	2.93
B. Wind	D	-1.36	1.49	-2.07	2.05	-2.34	2.28	-3.30	2.83	-3.75	3.02	-4.02	3.39
	PS	-0.39	2.60	-0.91	2.73	-1.34	3.00	-2.12	4.16	-2.73	4.46	-3.10	4.55
C. CAS Deceleration	D	0.00	0.00	-0.01	0.15	-0.11	0.49	-1.43	2.24	-2.88	3.79	-4.99	5.22
	PS	0.00	0.00	0.00	0.00	0.00	0.00	-0.94	1.84	-2.35	4.35	-3.50	5.57
D. Speed Conformance	D	-0.02	0.12	-0.22	1.66	-0.10	2.19	-0.16	2.91	0.01	3.19	0.10	3.36
	PS	0.32	0.97	1.45	4.52	1.39	5.72	0.73	6.81	1.03	6.53	0.97	6.67
E. En-route Target Mach	D	-1.64	4.27	-1.26	5.50	-1.14	5.72	-1.12	5.74	-1.12	5.74	-1.12	5.74
	PS	-8.34	16.18	-8.70	16.46	-7.76	16.02	-7.48	15.94	-7.48	15.94	-7.48	15.94
F. Atmosphere / Altitude	D	0.02	0.19	-0.25	0.37	-0.41	0.44	-0.90	0.56	-1.08	0.60	-1.29	0.63
	PS	0.03	0.55	-0.45	1.05	-0.78	1.34	-1.49	1.86	-1.87	2.09	-2.27	2.27
G. Path Distance	D	0.46	0.29	0.74	0.34	0.91	0.37	1.41	0.64	1.72	0.70	2.32	0.88
	PS	-8.21	4.87	-8.74	3.78	-8.62	3.80	-8.20	3.88	-7.79	3.92	-5.16	4.99
Total	D	-0.77	5.80	-3.92	6.70	-4.59	8.17	-7.50	8.87	-12.51	8.72	-15.65	9.88
	PS	-15.07	23.85	-16.97	26.33	-18.67	27.08	-23.89	26.49	-26.71	25.64	-26.99	25.78
Residual	D	0.11	1.27	-0.19	1.49	0.04	1.59	0.50	2.07	0.40	1.99	-0.57	2.49
	PS	1.12	2.34	0.41	1.77	0.80	1.49	1.31	1.45	0.50	2.21	-0.43	3.41

Acknowledgments

This research was funded by NASA Ames under contract NNA12AC09C.

References

[1]Coppenbarger, R., Hayashi, M., Nagle, G., Sweet, D., and Salcido, R., "The Efficient Descent Advisor: Technology Validation and Transition", *12th AIAA Aviation Technology, Integration, and Operations (ATIO) Conference*, Indianapolis, IN, September 17-19, 2012.

[2]Coppenbarger, R.A., Lanier, R., Sweet, D., and Dorsky, S., "Design and Development of the En Route Descent Advisor (EDA) for Conflict-Free Arrival Metering", *AIAA Guidance, Navigation, and Control (GNC) Conference*, Providence, RI, August, 2004.

[3]Coppenbarger, R., Dyer, G., Hayashi, M., Lanier, R., Stell, L., and Sweet, D., "Development and Testing of Automation for Efficient Arrivals in Constrained Airspace", *27th International Congress of the Aeronautical Sciences (ICAS)*, Nice, France, 2010.

[4]Green, S.M., and Vivona, R.A., "En Route Descent Advisor Concept for Arrival Metering", *AIAA Guidance, Navigation, and Control (GNC) Conference*, Montreal, Canada, August 6-9, 2001.

[5]Haraldsdottir, A., Scharl, J., Berge, M.E., Schoemig, E.G., and Coats, M.L., "Arrival Management with Required Navigation Performance and 3D Paths", *7th USA/Europe Air Traffic Management Research and Development Seminar*, Barcelona, Spain, 2007.

[6]Schoemig, E.G., Armbruster, J., Boyle, D.E., and Haraldsdottir, A., "3D Path Concept and Flight Management System (FMS) Trades", *25th Digital Avionics System Conference*, Portland, Oregon, October 2006.

[7]Nagle, G., Sweet, D., Carr, G., Felipe, V., Trapani, A., Coppenbarger, R., and Hayashi, M., "Human-in-the-Loop Simulation of Three-Dimensional Path Arrival Management with Trajectory Error", *11th AIAA Aviation Technology, Integration, and Operations (ATIO) Conference*, Virginia Beach, VA, September 20-22, 2011.

[8]Green, S., and Vivona, R., "Field Evaluation of Descent Advisor Trajectory Prediction Accuracy", *AIAA Guidance, Navigation, and Control Conference*, San Diego, CA, July 1996.

[9]Green, S.M., Vivona, R.A., Grace, M.P., and Fang, T.-C., "Field Evaluation of Descent Advisor Trajectory Prediction Accuracy for En-route Clearance Advisories", *AIAA Guidance, Navigation, and Control (GNC) Conference*, 1998.

[10]Green, S., Grace, M.P., and Williams, D.H., "Flight Test Results: CTAS and FMS Cruise/Descent Trajectory Prediction Accuracy", *3rd USA/Europe Air Traffic Management Research and Development Seminar*, Napoli, Italy, June 3-6, 2000.

[11]Slattery, R., and Zhao, Y., "En-route Descent Trajectory Synthesis for Air Traffic Control Automation", *Proceedings of the American Control Conference*, vol. 5, June 1995, pp. 3430-3434.

[12]Slattery, R., and Zhao, Y., "Trajectory Synthesis for Air Traffic Automation", *Journal of Guidance, Control, and Dynamics*, vol. 20, no. 2, March 1997, pp. 232-238.

[13]Lee, A.G., Bouyssounouse, X., and Murphy, J.R., "The Trajectory Synthesizer Generalized Profile Interface", *10th AIAA Aviation Technology, Integration and Operations (ATIO) Conference*, Fort Worth, Texas, September 13-15, 2010.

[14]Wu, M.G., and Green, S.M., "Strategies for Choosing Descent Flight-Path Angles for Small Jets", *AIAA Guidance, Navigation, and Control Conference*, Minneapolis, MN, August 13-16, 2012.

[15]Wu, M.G., and Green, S.M., "Choosing Descent Flight-Path Angles for Small Jets: Adaptation to the JFK Airport", *AIAA Aviation Technology, Integration, and Operations (ATIO) Conference*, Los Angeles, CA, August 12-14, 2013.

[16]Ryan, H.F., Paglione, M.M., and Green, S.M., "Review of Trajectory Accuracy Methodology and Comparison of Error Measurement Metrics", *AIAA Guidance, Navigation, and Control (GNC) Conference*, Providence, RI, August, 2004.

[17]Green, S.M., Henderson, J., Vivona, R., and Wu, G., "Trajectory Prediction Accuracy and Error Sources for Regional Jet Descents: Results of 2010 FAA Global 5000 Flight Trial at Denver International Airport", Unpublished Manuscript, 2013.

[18]Cole, R.E., Green, S., Jardin, M., Schwartz, B.E., and Benjamin, S.G.., "Wind Prediction Accuracy for Air Traffic Management Decision Support Tools", *3rd USA/Europe Air Traffic Management Research and Development Seminar*, Napoli, Italy, June 3-6, 2000.